ELSEVIER

Total cross section in $\gamma\gamma$ collisions at LEP

L3 Collaboration

M. Acciarri [y], P. Achard [s], O. Adriani [p], M. Aguilar-Benitez [x], J. Alcaraz [x],
G. Alemanni [u], J. Allaby [q], A. Aloisio [aa], M.G. Alviggi [aa], G. Ambrosi [s], H. Anderhub [au],
V.P. Andreev [f,af], T. Angelescu [l], F. Anselmo [i], A. Arefiev [z], T. Azemoon [c], T. Aziz [j],
P. Bagnaia [ak], A. Bajo [x], L. Baksay [ap], A. Balandras [d], S.V. Baldew [b], S. Banerjee [j],
Sw. Banerjee [d], A. Barczyk [au,as], R. Barillère [q], P. Bartalini [u], M. Basile [i], N. Batalova [ar],
R. Battiston [ae], A. Bay [u], F. Becattini [p], U. Becker [n], F. Behner [au], L. Bellucci [p],
R. Berbeco [c], J. Berdugo [x], P. Berges [n], B. Bertucci [ae], B.L. Betev [au], S. Bhattacharya [j],
M. Biasini [ae], A. Biland [au], J.J. Blaising [d], S.C. Blyth [ag], G.J. Bobbink [b], A. Böhm [a],
L. Boldizsar [m], B. Borgia [ak], D. Bourilkov [au], M. Bourquin [s], S. Braccini [s],
J.G. Branson [am], F. Brochu [d], A. Buffini [p], A. Buijs [aq], J.D. Burger [n], W.J. Burger [ae],
X.D. Cai [n], M. Capell [n], G. Cara Romeo [i], G. Carlino [aa], A.M. Cartacci [p], J. Casaus [x],
G. Castellini [p], F. Cavallari [ak], N. Cavallo [ah], C. Cecchi [ae], M. Cerrada [x], F. Cesaroni [v],
M. Chamizo [s], Y.H. Chang [aw], U.K. Chaturvedi [r], M. Chemarin [w], A. Chen [aw], G. Chen [g],
G.M. Chen [g], H.F. Chen [t], H.S. Chen [g], G. Chiefari [aa], L. Cifarelli [al], F. Cindolo [i],
C. Civinini [p], I. Clare [n], R. Clare [aj], G. Coignet [d], N. Colino [x], S. Costantini [e],
F. Cotorobai [l], B. de la Cruz [x], A. Csilling [m], S. Cucciarelli [ae], T.S. Dai [n],
J.A. van Dalen [ac], R. D'Alessandro [p], R. de Asmundis [aa], P. Déglon [s], A. Degré [d],
K. Deiters [as], D. della Volpe [aa], E. Delmeire [s], P. Denes [ai], F. DeNotaristefani [ak],
A. De Salvo [au], M. Diemoz [ak], M. Dierckxsens [b], D. van Dierendonck [b], C. Dionisi [ak],
M. Dittmar [au], A. Dominguez [am], A. Doria [aa], M.T. Dova [r,5], D. Duchesneau [d],
D. Dufournaud [d], P. Duinker [b], H. El Mamouni [w], A. Engler [ag], F.J. Eppling [n],
F.C. Erné [b], A. Ewers [a], P. Extermann [s], M. Fabre [as], M.A. Falagan [x], S. Falciano [ak,q],
A. Favara [q], J. Fay [w], O. Fedin [af], M. Felcini [au], T. Ferguson [ag], H. Fesefeldt [a],
E. Fiandrini [ae], J.H. Field [s], F. Filthaut [q], P.H. Fisher [n], I. Fisk [am], G. Forconi [n],
K. Freudenreich [au], C. Furetta [y], Yu. Galaktionov [z,n], S.N. Ganguli [j], P. Garcia-Abia [e],
M. Gataullin [ad], S.S. Gau [k], S. Gentile [ak,q], N. Gheordanescu [l], S. Giagu [ak], Z.F. Gong [t],
G. Grenier [w], O. Grimm [au], M.W. Gruenewald [h], M. Guida [al], R. van Gulik [b],
V.K. Gupta [ai], A. Gurtu [j], L.J. Gutay [ar], D. Haas [e], A. Hasan [ab], D. Hatzifotiadou [i],
T. Hebbeker [h], A. Hervé [q], P. Hidas [m], J. Hirschfelder [ag], H. Hofer [au], G. Holzner [au],

H. Hoorani [ag], S.R. Hou [aw], Y. Hu [ac], I. Iashvili [at], B.N. Jin [g], L.W. Jones [c], P. de Jong [b], I. Josa-Mutuberría [x], R.A. Khan [r], D. Käfer [a], M. Kaur [r,6], M.N. Kienzle-Focacci [s], D. Kim [ak], J.K. Kim [ao], J. Kirkby [q], D. Kiss [m], W. Kittel [ac], A. Klimentov [n,z], A.C. König [ac], M. Kopal [ar], A. Kopp [at], V. Koutsenko [n,z], M. Kräber [au], R.W. Kraemer [ag], W. Krenz [a], A. Krüger [at], A. Kunin [n,z], P. Ladron de Guevara [x], I. Laktineh [w], G. Landi [p], M. Lebeau [q], A. Lebedev [n], P. Lebrun [w], P. Lecomte [au], P. Lecoq [q], P. Le Coultre [au], H.J. Lee [h], J.M. Le Goff [q], R. Leiste [at], P. Levtchenko [af], C. Li [t], S. Likhoded [at], C.H. Lin [aw], W.T. Lin [aw], F.L. Linde [b], L. Lista [aa], Z.A. Liu [g], W. Lohmann [at], E. Longo [ak], Y.S. Lu [g], K. Lübelsmeyer [a], C. Luci [q,ak], D. Luckey [n], L. Lugnier [w], L. Luminari [ak], W. Lustermann [au], W.G. Ma [t], M. Maity [j], L. Malgeri [s], A. Malinin [q], C. Maña [x], D. Mangeol [ac], J. Mans [ai], G. Marian [o], J.P. Martin [w], F. Marzano [ak], K. Mazumdar [j], R.R. McNeil [f], S. Mele [q], L. Merola [aa], M. Meschini [p], W.J. Metzger [ac], M. von der Mey [a], A. Mihul [l], H. Milcent [q], G. Mirabelli [ak], J. Mnich [a], G.B. Mohanty [j], T. Moulik [j], G.S. Muanza [w], A.J.M. Muijs [b], B. Musicar [am], M. Musy [ak], M. Napolitano [aa], F. Nessi-Tedaldi [au], H. Newman [ad], T. Niessen [a], A. Nisati [ak], H. Nowak [at], R. Ofierzynski [au], G. Organtini [ak], A. Oulianov [z], C. Palomares [x], D. Pandoulas [a], S. Paoletti [ak,q], P. Paolucci [aa], R. Paramatti [ak], H.K. Park [ag], I.H. Park [ao], G. Passaleva [q], S. Patricelli [aa], T. Paul [k], M. Pauluzzi [ae], C. Paus [q], F. Pauss [au], M. Pedace [ak], S. Pensotti [y], D. Perret-Gallix [d], B. Petersen [ac], D. Piccolo [aa], F. Pierella [i], M. Pieri [p], P.A. Piroué [ai], E. Pistolesi [y], V. Plyaskin [z], M. Pohl [s], V. Pojidaev [z,p], H. Postema [n], J. Pothier [q], D.O. Prokofiev [ar], D. Prokofiev [af], J. Quartieri [al], G. Rahal-Callot [au,q], M.A. Rahaman [j], P. Raics [o], N. Raja [j], R. Ramelli [au], P.G. Rancoita [y], R. Ranieri [p], A. Raspereza [at], G. Raven [am], P. Razis [ab], D. Ren [au], M. Rescigno [ak], S. Reucroft [k], S. Riemann [at], K. Riles [c], J. Rodin [ap], B.P. Roe [c], L. Romero [x], A. Rosca [h], S. Rosier-Lees [d], S. Roth [a], C. Rosenbleck [a], B. Roux [ac], J.A. Rubio [q], G. Ruggiero [p], H. Rykaczewski [au], S. Saremi [f], S. Sarkar [ak], J. Salicio [q], E. Sanchez [q], M.P. Sanders [ac], C. Schäfer [q], V. Schegelsky [af], S. Schmidt-Kaerst [a], D. Schmitz [a], H. Schopper [av], D.J. Schotanus [ac], G. Schwering [a], C. Sciacca [aa], A. Seganti [i], L. Servoli [ae], S. Shevchenko [ad], N. Shivarov [an], V. Shoutko [z], E. Shumilov [z], A. Shvorob [ad], T. Siedenburg [a], D. Son [ao], B. Smith [ag], P. Spillantini [p], M. Steuer [n], D.P. Stickland [ai], A. Stone [f], B. Stoyanov [an], A. Straessner [q], K. Sudhakar [j], G. Sultanov [r], L.Z. Sun [t], S. Sushkov [h], H. Suter [au], J.D. Swain [r], Z. Szillasi [ap,3], T. Sztaricskai [ap,3], X.W. Tang [g], L. Tauscher [e], L. Taylor [k], B. Tellili [w], D. Teyssier [w], C. Timmermans [ac], Samuel C.C. Ting [n], S.M. Ting [n], S.C. Tonwar [j], J. Tóth [m], C. Tully [q], K.L. Tung [g], Y. Uchida [n], J. Ulbricht [au], E. Valente [ak], G. Vesztergombi [m], I. Vetlitsky [z], D. Vicinanza [al], G. Viertel [au], S. Villa [aj], M. Vivargent [d], S. Vlachos [e], I. Vodopianov [af], H. Vogel [ag], H. Vogt [at], I. Vorobiev [ag], A.A. Vorobyov [af], A. Vorvolakos [ab], M. Wadhwa [e], W. Wallraff [a], M. Wang [n], X.L. Wang [t], Z.M. Wang [t], A. Weber [a], M. Weber [a], P. Wienemann [a], H. Wilkens [ac], S.X. Wu [n], S. Wynhoff [q], L. Xia [ad], Z.Z. Xu [t],

J. Yamamoto [c], B.Z. Yang [t], C.G. Yang [g], H.J. Yang [g], M. Yang [g], J.B. Ye [t], S.C. Yeh [ax],
An. Zalite [af], Yu. Zalite [af], Z.P. Zhang [t], G.Y. Zhu [g], R.Y. Zhu [ad], A. Zichichi [i,q,r],
G. Zilizi [ap,3], B. Zimmermann [au], M. Zöller [a]

[a] *I. Physikalisches Institut, RWTH, D-52056 Aachen, FRG* [1]
and III. Physikalisches Institut, RWTH, D-52056 Aachen, FRG [1]
[b] *National Institute for High Energy Physics, NIKHEF,*
and University of Amsterdam, NL-1009 DB Amsterdam, The Netherlands
[c] *University of Michigan, Ann Arbor, MI 48109, USA*
[d] *Laboratoire d'Annecy-le-Vieux de Physique des Particules, LAPP, IN2P3-CNRS, BP 110, F-74941 Annecy-le-Vieux Cedex, France*
[e] *Institute of Physics, University of Basel, CH-4056 Basel, Switzerland*
[f] *Louisiana State University, Baton Rouge, LA 70803, USA*
[g] *Institute of High Energy Physics, IHEP, 100039 Beijing, China* [7]
[h] *Humboldt University, D-10099 Berlin, FRG* [1]
[i] *University of Bologna and INFN, Sezione di Bologna, I-40126 Bologna, Italy*
[j] *Tata Institute of Fundamental Research, Bombay 400 005, India*
[k] *Northeastern University, Boston, MA 02115, USA*
[l] *Institute of Atomic Physics and University of Bucharest, R-76900 Bucharest, Romania*
[m] *Central Research Institute for Physics of the Hungarian Academy of Sciences, H-1525 Budapest 114, Hungary* [2]
[n] *Massachusetts Institute of Technology, Cambridge, MA 02139, USA*
[o] *KLTE-ATOMKI, H-4010 Debrecen, Hungary* [3]
[p] *INFN Sezione di Firenze and University of Florence, I-50125 Florence, Italy*
[q] *European Laboratory for Particle Physics, CERN, CH-1211 Geneva 23, Switzerland*
[r] *World Laboratory, FBLJA Project, CH-1211 Geneva 23, Switzerland*
[s] *University of Geneva, CH-1211 Geneva 4, Switzerland*
[t] *Chinese University of Science and Technology, USTC, Hefei, Anhui 230 029, China* [7]
[u] *University of Lausanne, CH-1015 Lausanne, Switzerland*
[v] *INFN, Sezione di Lecce and Università Degli Studi di Lecce, I-73100 Lecce, Italy*
[w] *Institut de Physique Nucléaire de Lyon, IN2P3-CNRS,Université Claude Bernard, F-69622 Villeurbanne, France*
[x] *Centro de Investigaciones Energéticas, Medioambientales y Tecnologícas, CIEMAT, E-28040 Madrid, Spain* [4]
[y] *INFN, Sezione di Milano, I-20133 Milan, Italy*
[z] *Institute of Theoretical and Experimental Physics, ITEP, Moscow, Russia*
[aa] *INFN, Sezione di Napoli and University of Naples, I-80125 Naples, Italy*
[ab] *Department of Natural Sciences, University of Cyprus, Nicosia, Cyprus*
[ac] *University of Nijmegen and NIKHEF, NL-6525 ED Nijmegen, The Netherlands*
[ad] *California Institute of Technology, Pasadena, CA 91125, USA*
[ae] *INFN, Sezione di Perugia and Università Degli Studi di Perugia, I-06100 Perugia, Italy*
[af] *Nuclear Physics Institute, St. Petersburg, Russia*
[ag] *Carnegie Mellon University, Pittsburgh, PA 15213, USA*
[ah] *INFN, Sezione di Napoli and University of Potenza, I-85100 Potenza, Italy*
[ai] *Princeton University, Princeton, NJ 08544, USA*
[aj] *University of Californa, Riverside, CA 92521, USA*
[ak] *INFN, Sezione di Roma and University of Rome, "La Sapienza", I-00185 Rome, Italy*
[al] *University and INFN, Salerno, I-84100 Salerno, Italy*
[am] *University of California, San Diego, CA 92093, USA*
[an] *Bulgarian Academy of Sciences, Central Lab. of Mechatronics and Instrumentation, BU-1113 Sofia, Bulgaria*
[ao] *Laboratory of High Energy Physics, Kyungpook National University, 702-701 Taegu, South Korea*
[ap] *University of Alabama, Tuscaloosa, AL 35486, USA*
[aq] *Utrecht University and NIKHEF, NL-3584 CB Utrecht, The Netherlands*
[ar] *Purdue University, West Lafayette, IN 47907, USA*
[as] *Paul Scherrer Institut, PSI, CH-5232 Villigen, Switzerland*
[at] *DESY, D-15738 Zeuthen, FRG*
[au] *Eidgenössische Technische Hochschule, ETH Zürich, CH-8093 Zürich, Switzerland*
[av] *University of Hamburg, D-22761 Hamburg, FRG*
[aw] *National Central University, Chung-Li, Taiwan, ROC*
[ax] *Department of Physics, National Tsing Hua University, Taiwan, ROC*

Abstract

The reaction $e^+e^- \to e^+e^-\gamma^*\gamma^* \to e^+e^-$ *hadrons* for quasi-real photons is studied using data from $\sqrt{s} = 183$ GeV up to 202 GeV. Results on the total cross sections $\sigma(e^+e^- \to e^+e^-$ *hadrons*) and $\sigma(\gamma\gamma \to$ *hadrons*) are given for the two-photon centre-of-mass energies 5 GeV $\leqslant W_{\gamma\gamma} \leqslant 185$ GeV. The total cross section of two real photons is described by a Regge parametrisation. We observe a steeper rise with the two-photon centre-of-mass energy as compared to the hadron–hadron and the photon–proton cross sections. The data are also compared to the expectations of different theoretical models.
© 2001 Published by Elsevier Science B.V.

1. Introduction

At high centre-of-mass energies, $\sqrt{s}$, the two-photon process $e^+e^- \to e^+e^-\gamma^*\gamma^* \to e^+e^-$ *hadrons* is a copious source of hadron production. Most of the initial energy is taken by the scattered electrons.[8] As their scattering angle is low, they often go undetected. The hadron system has, typically, a low mass compared to $\sqrt{s}$. A large fraction of the hadrons escape detection, due to the Lorentz boost of the $\gamma\gamma$ system and to the large diffractive cross section producing hadrons at small polar angles, where the detector acceptance is limited. For these reasons, the measured visible mass, W_{vis}, is less than the two photon effective mass, $W_{\gamma\gamma}$.

In this Letter we analyse only data where the scattered electrons are not detected. New results on total cross sections $\sigma(e^+e^- \to e^+e^-$ *hadrons*) are presented, using data collected with the L3 detector

[1] for a total integrated luminosity of 51.4 pb^{-1} at $\sqrt{s} = 183$ GeV, 171.8 pb^{-1} at $\sqrt{s} = 189$ GeV and 220.8 pb^{-1} at $\sqrt{s} = 192, 196, 200, 202$ GeV.

The two-photon cross section $\sigma(\gamma\gamma \to$ *hadrons*) is derived in the interval 5 GeV $\leqslant W_{\gamma\gamma} \leqslant 185$ GeV, while the analysis of the data taken at $\sqrt{s} = 133$ and 161 GeV [2] covered only the interval 5 GeV $\leqslant W_{\gamma\gamma} \leqslant 75$ GeV.

2. Measurement of cross sections

2.1. Monte Carlo simulation

The $e^+e^- \to e^+e^-\gamma^*\gamma^* \to e^+e^-$ *hadrons* processes are generated with the PHOJET [3] and PYTHIA [4] event generators. For the annihilation process $e^+e^- \to q\bar{q}(\gamma)$, PYTHIA is used. KORALZ [5] is used for $e^+e^- \to \tau^+\tau^-(\gamma)$ and KORALW [6] for $e^+e^- \to W^+W^-$. The $e^+e^- \to e^+e^-\tau^+\tau^-$ channel is generated by DIAG36 [7]. The Monte Carlo events are simulated in the L3 detector using the GEANT [8] and GHEISHA [9] programs and passed through the same reconstruction program as the data. Time dependent detector inefficiencies, as monitored during the data taking period, are also simulated.

2.2. Event selection

The analysis is based on the central tracking system, the high resolution electromagnetic calorimeter, the hadron calorimeter and the luminosity monitor.

Two-photon events are collected predominantly by the track triggers [10]. The trigger efficiency is studied

[8] Electron stands for electron and positron throughout this Letter.

separately for each data sample by comparing the number of events accepted by the track trigger and the calorimetric energy trigger. The efficiencies of higher level triggers are measured using prescaled events. The trigger efficiency increases from 80% at $W_{\text{vis}} = 5$ GeV to 94% above 80 GeV.

Hadronic two-photon events are selected by the following criteria:

- To exclude scattered electrons, events with clusters in the luminosity monitor having energy greater

than 30 GeV, in a fiducial region of 33 mrad $\leqslant \theta \leqslant 64$ mrad are rejected. The virtuality of the interacting photons, Q^2, is thus less than 8 GeV^2, with an average value $\langle Q^2 \rangle \sim 1.5 \times 10^{-2}$ GeV^2. The distribution of low energy clusters in the luminosity monitor, presented in Fig. 1(a), shows a good agreement with both Monte Carlo programs. When the scattered electron reaches the detector, the agreement is maintained with the PHOJET Monte Carlo, while these configurations are missing
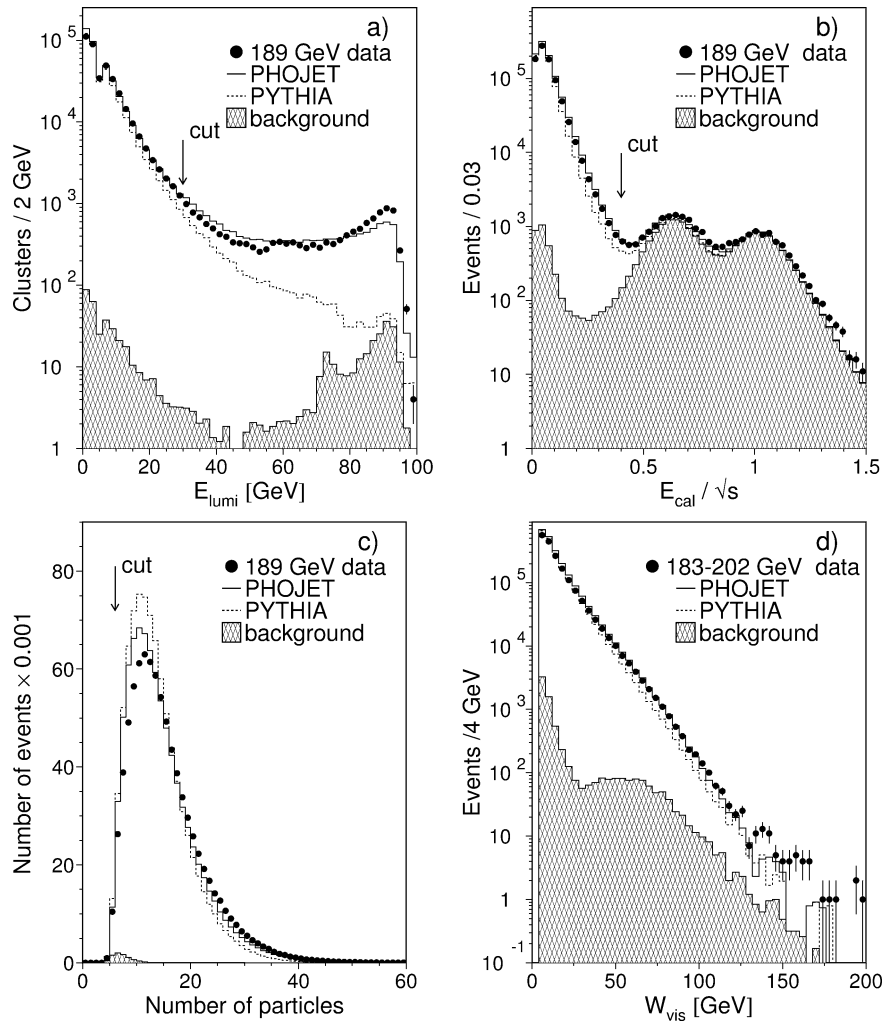

Fig. 1. Example of the distributions used for the event selection: (a) energy in the luminosity monitor; (b) energy E_{cal} in the electromagnetic and hadronic calorimeters, normalised to $\sqrt{s}$; (c) number of particles measured in the detector; (d) the distribution of the visible mass W_{vis}, for the full data sample at $\sqrt{s} = 183$–202 GeV. The data are compared with Monte Carlo predictions. The backgrounds due to e$^+$e$^-$ annihilation and e$^+$e$^- \to$ e$^+$e$^- \tau^+\tau^-$ are indicated as a shaded area.
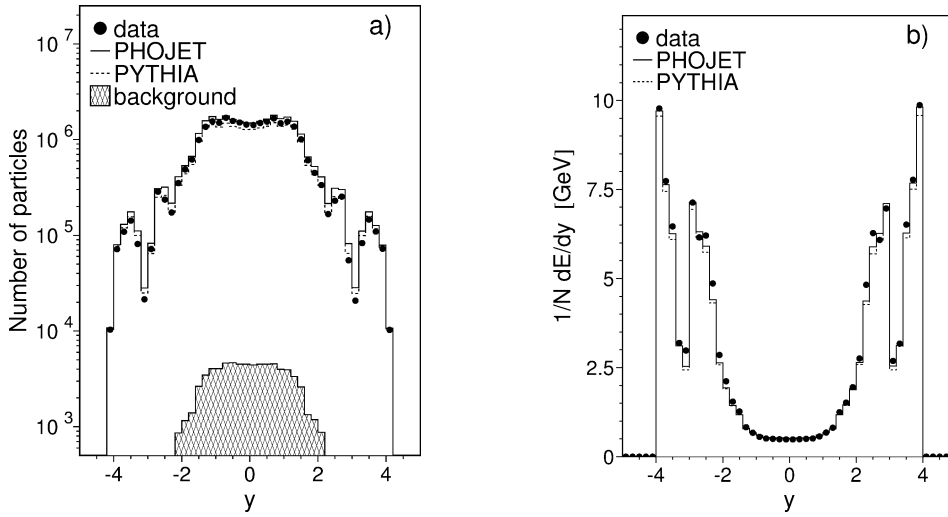
Fig. 2. (a) The distribution and (b) the average energy of the measured particles as a function of the rapidity y, for the full data sample at $\sqrt{s} = 183\text{–}202$ GeV. The data are compared with Monte Carlo predictions. The backgrounds due to e^+e^- annihilation and $e^+e^- \to e^+e^-\tau^+\tau^-$ are indicated as a shaded area.

in PYTHIA because of a ρ-mass cutoff, $Q^2 \leqslant m_\rho^2$, applied to the two-photon luminosity function in the generation of the events.

- The total energy in the electromagnetic calorimeter is required to be greater than 0.5 GeV, in order to suppress beam–gas and beam–wall backgrounds, and less than 50 GeV, to exclude radiative events, $e^+e^- \to Z\gamma$. The total energy deposited in the electromagnetic and hadronic calorimeters, E_{cal}, must be less than 40% of $\sqrt{s}$, to exclude annihilation events, as shown in Fig. 1(b).
- At least six particles must be detected, in order to exclude events containing τ. A particle is defined [2] as either a track, a photon in the electromagnetic calorimeter, or a cluster in the hadron calorimeter or in the luminosity monitor. Clusters in the luminosity monitor are considered as pions if their energy is below 5 GeV, as photons otherwise. The distribution of the number of particles is presented in Fig. 1(c). This distribution is not well reproduced by the Monte Carlo simulations.

After selection, the background from beam–gas and beam–wall interactions is found to be negligible. The visible effective mass of the event, W_{vis}, is calculated from the four-momenta of the measured particles. The analysis is limited to events with $W_{\text{vis}} \geqslant 5$ GeV.

Almost 2 million events are selected, 1.6×10^5 at $\sqrt{s} = 183$ GeV, 7.8×10^5 at $\sqrt{s} = 189$ GeV and 1×10^6 at $\sqrt{s} = 192\text{–}202$ GeV. The average centre-of-mass energy of this last sample is $\sqrt{s} = 198$ GeV.

The W_{vis} spectrum is shown in Fig. 1(d) for the total data sample. The background is below 1% at low masses, where it is dominated by two-photon τ-pair production. It increases at high masses, due mainly to annihilation processes and reaches a maximum of 15%.

The distributions of the rapidity, y, of the particles and of their energy flow are compared to the Monte Carlo expectations in Fig. 2. A good agreement is observed also in the regions where $|y| \simeq 3$, between the luminosity monitor and the hadron calorimeter.

2.3. Unfolding and efficiency

The distribution of the two-photon effective mass $W_{\gamma\gamma}$ is obtained from the visible effective mass W_{vis} by the same unfolding procedure [11] used in Ref. [2]. For each data sample, the W_{vis} spectrum is subdivided in 16 intervals, presented in Fig. 3(a), and the resulting $W_{\gamma\gamma}$ distribution in 8 intervals, presented in Fig. 3(b).
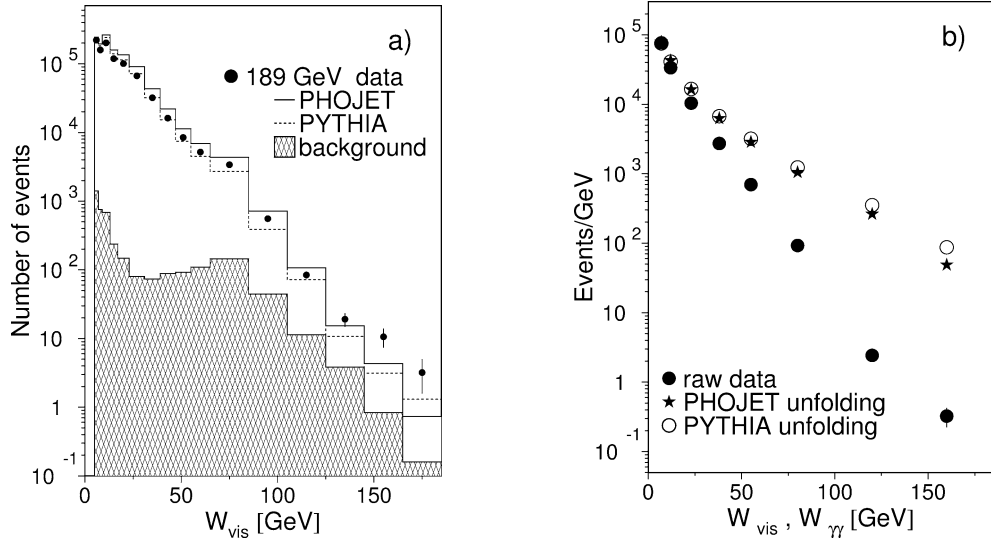
Fig. 3. Example of the unfolding for data at $\sqrt{s} = 189$ GeV. (a) Distribution of the measured visible mass W_{vis} in the 16 bins used for the unfolding. (b) The measured W_{vis} and the resulting $W_{\gamma\gamma}$ spectra, obtained by unfolding from W_{vis} to $W_{\gamma\gamma}$ with the Monte Carlo PHOJET or PYTHIA.

The result of the unfolding procedure depends on the Monte Carlo used. Data unfolded with PYTHIA are in general higher than if unfolded with PHOJET. After unfolding, the events are corrected for the efficiency, using the ratio between selected and generated events in each $W_{\gamma\gamma}$ interval. This includes the purely geometrical acceptance as well as the efficiencies of the detector and the analysis procedure. For $W_{\gamma\gamma} > 30$ GeV, the efficiency is rather constant, with a value of about 80%. The efficiency obtained with PYTHIA is lower by about 10%, which may be attributed to a different modeling of the diffractive interactions, in regions where particle detection is difficult.

2.4. Cross section determinations

The measured cross sections $\Delta\sigma(e^+e^- \to e^+e^-$ *hadrons*$)$ are given in Table 1 for the three data sets, as a function of the $W_{\gamma\gamma}$ intervals. The average of the results obtained by unfolding the data with PYTHIA or PHOJET is used. Due to the unfolding procedure, the measurements are highly correlated. The correlation matrix, similar for the three data sets, is given in Table 2 for $\sqrt{s} = 189$ GeV. The differential cross section $\Delta\sigma/\Delta W_{\gamma\gamma}$ is shown in Fig. 4, together with our measurements at lower LEP
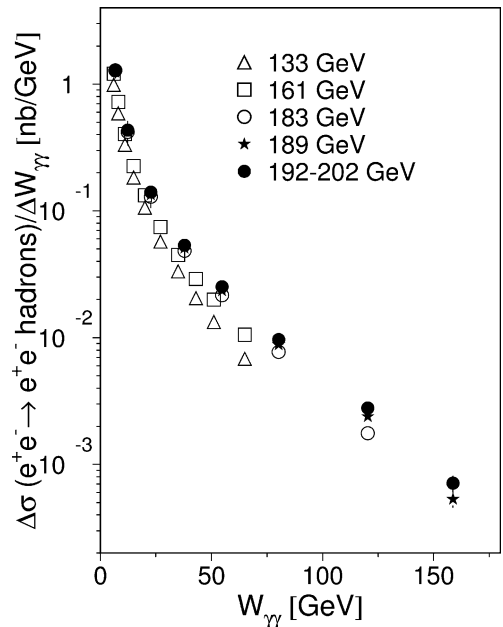

Fig. 4. The cross section $\Delta\sigma(e^+e^- \to e^+e^-$ *hadrons*$)/\Delta W_{\gamma\gamma}$ measured at $\sqrt{s} = 133$–202 GeV. Statistical and systematic uncertainties are added in quadrature and are often smaller than the symbol size.

Table 1
The measured cross sections $\Delta\sigma(e^+e^- \to e^+e^-\ hadrons)$ as a function of the $\gamma\gamma$ centre-of-mass energy $W_{\gamma\gamma}$ for the three data sets. Only the statistical uncertainties, obtained after unfolding, are given

$\Delta W_{\gamma\gamma}$ (GeV)	$\langle W_{\gamma\gamma} \rangle$ (GeV)	$\sqrt{s} = 183$ GeV $\Delta\sigma_{e^+e^-}$ (nb)	$\sqrt{s} = 189$ GeV $\Delta\sigma_{e^+e^-}$ (nb)	$\sqrt{s} = 198$ GeV $\Delta\sigma_{e^+e^-}$ (nb)
5–9	6.7	5.145 ± 0.025	4.996 ± 0.009	5.093 ± 0.008
9–17	12.3	3.358 ± 0.013	3.350 ± 0.006	3.466 ± 0.005
17–31	22.7	1.812 ± 0.007	1.880 ± 0.004	1.962 ± 0.003
31–47	37.8	0.776 ± 0.004	0.813 ± 0.002	0.857 ± 0.002
47–65	54.8	0.388 ± 0.003	0.422 ± 0.002	0.453 ± 0.002
65–105	80.2	0.308 ± 0.003	0.353 ± 0.002	0.386 ± 0.001
105–145	120.4	0.070 ± 0.001	0.096 ± 0.001	0.111 ± 0.001
145–185	158.7	–	0.021 ± 0.001	0.028 ± 0.001

Table 2
The correlation matrix after unfolding, for the data taken at $\sqrt{s} = 189$ GeV

$\Delta W_{\gamma\gamma}$ (GeV)	5–9	9–17	17–31	31–47	47–65	65–105	105–145	145–185
5–9	1.0							
9–17	0.931	1.0						
17–31	0.815	0.939	1.0					
31–47	0.692	0.803	0.908	1.0				
47–65	0.525	0.602	0.689	0.761	1.0			
65–105	0.336	0.384	0.436	0.497	0.486	1.0		
105–145	0.130	0.150	0.166	0.186	0.190	0.208	1.0	
145–185	0.063	0.072	0.077	0.080	0.077	0.089	0.094	1.0

collision energies [2]. The fast decrease of the cross section as a function of $W_{\gamma\gamma}$ is due to the two photon luminosity function, $\mathcal{L}_{\gamma\gamma}$, which depends on $W_{\gamma\gamma}^2/s$.

The systematic uncertainties are evaluated for each $W_{\gamma\gamma}$ bin. They are independent of the data sample, inside statistical accuracy. They are evaluated as follows and their contribution is listed in Table 3.

- Trigger efficiencies: by varying this quantity within the accuracy of its determination, of about 10%.
- Energy scale of the calorimeters and contribution of the annihilation background: by varying the E_{cal} cut by $\pm 10\%$ of $\sqrt{s}$.
- Uncertainties on the rejection of scattered electrons: by changing the E_{lumi} cut from 30 to 50 GeV.

- Uncertainties on the particle multiplicity: by accepting a minimum number of four or eight particles instead of six.
- Uncertainties due to Monte Carlo statistics are negligible for $W_{\gamma\gamma} < 65$ GeV, but important in the higher $W_{\gamma\gamma}$ bins.

Uncertainties on the energy scale of the small angle calorimeter, evaluated by varying the gain by a factor two, are negligible. The total experimental systematic uncertainty, obtained by adding in quadrature all contributions, is also given in Table 3. The uncertainty related to the Monte Carlo model is given in the last column of Table 3. It is half of the difference between the results obtained by unfolding the data with PHOJET

Table 3
Evaluation of systematic uncertainties due to the trigger, the analysis cuts and the Monte Carlo statistics. All values are per-cent uncertainties on the cross sections $\Delta\sigma(e^+e^- \to e^+e^-\ hadrons)$ and $\sigma(\gamma\gamma \to hadrons)$. The uncertainty introduced by unfolding the data with PYTHIA or PHOJET is considered separately in the last column. A further scale uncertainty of 5% must be added for the $\sigma(\gamma\gamma \to hadrons)$ cross sections, due to the two-photon luminosity function

$\Delta W_{\gamma\gamma}$ (GeV)	Trigger	E_{cal}	E_{lumi}	N_{part}	MC stat.	Total exp.	MC model
5–9	0.9	0.1	< 0.1	7.4	< 0.1	7.5	7.0
9–17	0.9	0.1	< 0.1	5.0	< 0.1	5.1	1.2
17–31	0.7	0.1	< 0.1	3.2	< 0.1	3.3	4.0
31–47	0.6	0.2	0.2	2.0	< 0.1	2.1	6.8
47–65	0.5	0.2	0.1	1.7	< 0.1	1.8	8.9
65–105	0.4	0.2	1.1	1.7	1.5	2.6	10.4
105–145	0.4	0.3	3.0	1.3	8.1	8.7	15.5
145–185	0.4	0.8	6.4	2.2	12.4	14.1	27.4

or PYTHIA and exceeds the experimental uncertainty in almost all bins.

To extract the total cross section of two real photons, the luminosity function $\mathcal{L}_{\gamma\gamma}$ [12] is calculated and the hadronic two-photon process is extrapolated to $Q^2 = 0$. This is done as in Ref. [2] by using an analytical program [13]. Depending on the choice of photon form factors, this calculation varies of $\pm 5\%$.

The cross sections obtained for the three data sets are compatible within the experimental uncertainties and are presented in Table 4. As expected from the study of the experimental systematics, the largest differences are observed in the first and last bins. The combined value is also given in Table 4 and in Fig. 5(a) with the statistical uncertainties obtained from the unfolding and the experimental systematics. The values obtained by unfolding the data with the two Monte Carlo programs separately are shown in Fig. 5(b) and can be obtained from the last column of Table 4.

Table 4
The $\sigma(\gamma\gamma \to hadrons)$ cross sections as a function of the average $\gamma\gamma$ centre-of-mass energy, $\langle W_{\gamma\gamma}\rangle$, for the three data sets and for their combination. The statistical uncertainties, obtained after unfolding, are given for each data set. The experimental systematic uncertainty, $\Delta\sigma_{\gamma\gamma}^{exp}$, and the difference, $\Delta\sigma_{\gamma\gamma}^{MC}$, between the average value and the result unfolded with PHOJET (lower sign) and with PYTHIA (upper sign) are also given. A further scale uncertainty of 5% must be added, due to the two-photon luminosity function

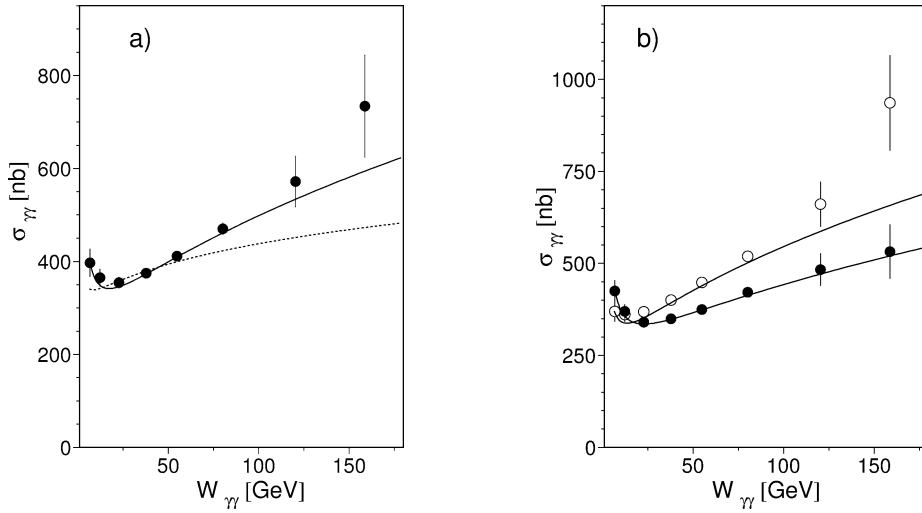| $\langle W_{\gamma\gamma}\rangle$ (GeV)	$\sqrt{s} = 183$ GeV $\sigma_{\gamma\gamma}$ (nb)	$\sqrt{s} = 189$ GeV $\sigma_{\gamma\gamma}$ (nb)	$\sqrt{s} = 198$ GeV $\sigma_{\gamma\gamma}$ (nb)	All data $\sigma_{\gamma\gamma}$ (nb)	$\Delta\sigma_{\gamma\gamma}^{exp}$ (nb)	$\Delta\sigma_{\gamma\gamma}^{MC}$ (nb)
6.7	422.6 ± 4.0	394.9 ± 0.7	398.4 ± 0.6	397.2 ± 0.5	30	∓ 28
12.3	378.4 ± 2.8	360.2 ± 0.7	368.2 ± 0.6	365.2 ± 0.4	19	∓ 4
22.7	359.8 ± 2.9	348.9 ± 0.7	358.2 ± 0.6	354.4 ± 0.5	12	± 14
37.8	382.1 ± 4.5	368.4 ± 1.1	379.2 ± 0.9	374.8 ± 0.8	8	± 26
54.8	408.6 ± 6.4	403.0 ± 1.8	418.0 ± 1.5	411.5 ± 1.1	7	± 37
80.2	461.2 ± 8.6	459.5 ± 2.2	478.5 ± 1.9	470.3 ± 1.4	13	± 49
120.4	496 ± 19	556.7 ± 5.3	586.1 ± 4.3	572.0 ± 3.3	53	± 89
158.7	–	726 ± 15	738 ± 11	734.1 ± 8.7	102	± 202

Fig. 5. The two-photon total cross section from the combined data at $\sqrt{s} = 183$–202 GeV. (a) The average result, obtained by unfolding the data with the two Monte Carlo models, is used. Two Regge fits, described in the text, are superimposed to the data. The continuous line corresponds to the fit with the coefficient ϵ left as a free parameter, the dashed line is the fit with ϵ fixed to 0.093. (b) The two-photon total cross section obtained by correcting the data sample with PHOJET (full points) and with PYTHIA (open points). The Regge fits of Table 5 are superimposed to the data. The statistical and experimental systematic uncertainties are added in quadrature.

3. Comparison with theoretical models

3.1. Regge parametrisation

The total cross sections for hadron–hadron, σ_{pp}, photon–hadron, $\sigma_{\gamma p}$, and photon–photon, $\sigma_{\gamma\gamma}$, production of hadrons show a characteristic steep decrease in the region of low centre-of-mass energy, followed by a slow rise at high energies [14]. From Regge theory [15] this behaviour is understood as the consequence of the exchange of Regge trajectories, $\alpha(t)$, in the t-channel. The total cross section takes the form $\sigma_{tot} \propto s^{\alpha(0)-1}$. The low energy region is sensitive to the exchange of a Reggeon R ($R = \rho, \omega, f, a, \ldots$), with $\alpha_R(0) \simeq 0.5$. At high energies, the Pomeron exchange dominates, with $\alpha_P(0) \simeq 1$. A parametrisation of the form

$$\sigma_{tot} = As^{\epsilon} + Bs^{-\eta} \tag{1}$$

accounts for the energy behaviour of all hadronic and photoproduction total cross sections, the powers of s being universal [16]. This is confirmed by the recent compilation of the total cross section data

[17] where a fit of Eq. (1) for all hadron total cross sections gives a result compatible with the universal values $\epsilon = 0.093 \pm 0.002$ and $\eta = 0.358 \pm 0.015$. The coefficients A and B are process and Q^2 dependent. If photons behave predominantly like hadrons, this expression may also be valid for the two-photon total hadronic cross section, with $s = W_{\gamma\gamma}^2$.

Considering only the experimental uncertainties, statistical and systematic, several Regge fits are performed on the data and their results are presented in Table 5. The exponent η is fixed to the universal value, since the low mass range is too small to be sensitive to this parameter. When the $W_{\gamma\gamma}$ interval is restricted to 5–65 GeV, a range similar to the one covered by our previous data [2], similar values of the parameters A and B are obtained. In this limited interval the data are compatible with the universal value of ϵ. Extending the range to the whole $W_{\gamma\gamma}$ interval, the fit with the exponents ϵ and η fixed to the universal value, dashed line in Fig. 5(a), does not represent the $\sigma_{\gamma\gamma}$ energy dependence. A fit with A, B and ϵ as free parameters, represented as a full line in Fig. 5(a), gives $\epsilon = 0.225 \pm 0.021$

Table 5
Fits to the total cross sections listed in Table 4 of the form $\sigma_{\gamma\gamma} = As^\epsilon + Bs^{-\eta}$ [16], where $s = W_{\gamma\gamma}^2$. PHOJET and PYTHIA indicates that only this Monte Carlo is used to unfold the data. In all other cases the average unfolding result of the two generators is used. The statistical and experimental uncertainties and the correlation matrix between the data points are used. The fitted parameters are strongly correlated. The second set of fits evaluates only the increase of $\sigma_{\gamma\gamma}$ with s, i.e., the Pomeron part of the fit. The values of the χ^2 and the corresponding confidence level are given

| Unfolding	$W_{\gamma\gamma}$ interval	A	B	η fixed	ϵ	χ^2/d.o.f.	C.L.
PHOJET	5–65 GeV	178 ± 5	453 ± 101	0.358	0.093 fixed	5.3/3	0.15
PYTHIA	5–185 GeV	181 ± 3	321 ± 120	0.358	0.093 fixed	55/6	10^{-9}
	5–185 GeV	58 ± 10	1020 ± 146	0.358	0.225 ± 0.021	12/5	0.04
	5–185 GeV	52 ± 11	1201 ± 146	0.358	0.221 ± 0.023	8.6/5	0.12
	5–185 GeV	63 ± 10	842 ± 146	0.358	0.228 ± 0.018	19/5	0.002
	17–105 GeV	165 ± 21	–	–	0.116 ± 0.016	4.3/2	0.12
	31–185 GeV	113 ± 19	–	–	0.163 ± 0.021	3.4/3	0.33
	47–185 GeV	81 ± 23	–	–	0.202 ± 0.035	1.5/2	0.48
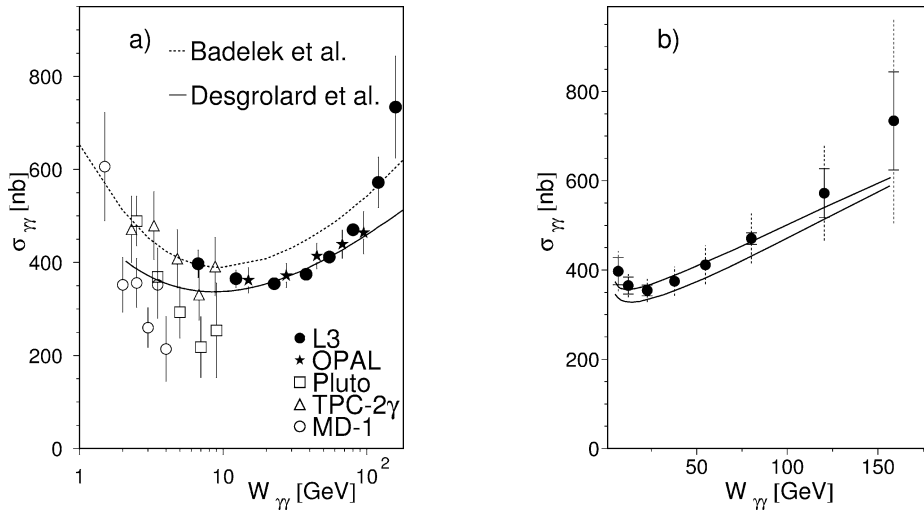
Fig. 6. The two-photon total cross sections compared to various models. (a) The predictions of Refs. [19,20] are compared to all two-photon total cross section data [21,23]. (b) Predictions of the minijet model [25]; the two lines correspond to different choices of the model parameters. The statistical and experimental systematic uncertainties are added in quadrature. The uncertainties due to Monte Carlo models and to the two-photon luminosity function are included in the dashed lines in (b).

with a confidence level of 4%. This value is more than a factor two higher than the universal value. It is independent of the Monte Carlo model used to correct the data, as shown in Table 5 and in Fig. 5(b).

The fitted value of ϵ is strongly correlated to the Reggeon component. To avoid this correlation, we fit only the Pomeron exchange for sufficiently high $W_{\gamma\gamma}$ values. The results, using a different initial value of $W_{\gamma\gamma}$, are listed in the second part of Table 5. The value of ϵ increases by increasing the lower mass cutoff, thus indicating that its value is not universal, but it reflects the onset of QCD phenomena, as ϵ increases with increasing $W_{\gamma\gamma}$.

3.2. Models for γγ total cross sections

Several models [18–20] were recently compared to the L3 and OPAL [21] measurements. Their predictions for the two-photon total cross section are typically derived from measurements of proton–proton and photoproduction total cross sections via the factorization relation: $\sigma_{\gamma\gamma} \approx \sigma_{\gamma p}^2 / \sigma_{pp}$ [22]. In general, these models give an energy dependence of the cross section similar to the universal fit discussed above. Two examples [19,20] are shown in Fig. 6(a) in comparison with the results of previous experiments [23], those presented in this Letter and those of OPAL. While the measurements at the low energy colliders present a wide spread, a good agreement is found between L3 and OPAL in the common $W_{\gamma\gamma}$ range, 10 GeV $\leqslant$ $W_{\gamma\gamma} \leqslant$ 110 GeV. Good agreement is also found if the data, unfolded separately with either PHOJET or PYTHIA, are compared. In this $W_{\gamma\gamma}$ region, a model [20] reproduces well the data and the predictions of the other [19] are too high by 20%. However, for both lower and higher values of $W_{\gamma\gamma}$, the L3 data show a much steeper energy dependence than the theoretical predictions.

In the Regge theory, the Pomeron intercept is 1, yielding a constant total cross section. When the rise of the proton–proton total cross section was first observed, it was explained [24] with an increase of the number of hard partonic interactions. The predictions of a model [25] that calculates such effects, using an eikonalized prescription to enforce unitarity, are shown in Fig. 6(b). The parameters of the model are determined from photoproduction data and the L3 results are well inside the uncertainty related to this extrapolation.

Models with two Pomerons were recently proposed [26] to explain the fast energy increase of charm production at HERA. In this model, the 'soft' and the 'hard' Pomeron have different intercepts. Because of the $q\bar{q}$ component in the photon wave-function, the 'hard' Pomeron can contribute to the two-photon cross section even at $Q^2 = 0$. Thus a more rapid energy dependence for $\sigma_{\gamma\gamma}$ is expected. The increase in ϵ with larger values of $W_{\gamma\gamma}$, as listed in the second part of Table 5, is consistent with such a contribution of the 'hard' Pomeron.

References

[1] L3 Collaboration, B. Adeva et al., Nucl. Instrum. Methods A 289 (1990) 35;
  M. Acciarri et al., Nucl. Instrum. Methods A 351 (1994) 300;
  M. Chemarin et al., Nucl. Instrum. Methods A 349 (1994) 345;
  A. Adam et al., Nucl. Instrum. Methods A 383 (1996) 342.
[2] L3 Collaboration, M. Acciari et al., Phys. Lett. B 408 (1997) 450.
[3] PHOJET version 1.05c is used;
  R. Engel, Z. Phys. C 66 (1995) 203;
  R. Engel, J. Ranft, Phys. Rev. D 54 (1996) 4246.
[4] PYTHIA version 5.722 and JETSET version 7.409 are used;
  T. Sjöstrand, Comput. Phys. Commun. 82 (1994) 74.
[5] KORALZ version 4.02 is used;
  S. Jadach, B.F.L. Ward, Z. Was, Comput. Phys. Commun. 79 (1994) 503.
[6] KORALW version 1.33 is used;
  M. Skrzypek et al., Comput. Phys. Commun. 94 (1996) 216.
[7] F.A. Berends, P.H. Daverfeldt, R. Kleiss, Nucl. Phys. B 253 (1985) 441.
[8] R. Brun et al., GEANT 3.15 preprint CERN DD/EE/84-1 (1984), revised 1987.
[9] H. Fesefeldt, RWTH Aachen report PITHA 85/2 (1985).
[10] P. Béné et al., Nucl. Instrum. Methods A 306 (1991) 150;
  D. Haas et al., Nucl. Instrum. Methods A 420 (1999) 101.
[11] G. D'Agostini, Nucl. Instrum. Methods A 362 (1995) 487.
[12] V.M. Budnev et al., Phys. Rep. C 15 (1975) 181.
[13] G.A. Schuler, hep-ph/9610406.
  We wish to thank the author for providing us with the numerical integration program of the luminosity function.
[14] J.J. Sakurai, D. Schildknecht, Phys. Lett. B 40 (1972) 121.
[15] P.D.B. Collins, Introduction to Regge theory, Cambridge Univ. Press, Cambridge, 1977.
[16] A. Donnachie, P.V. Landshoff, Phys. Lett. B 296 (1992) 227.
[17] D.E. Groom et al., Eur. Phys. J. C 15 (2000) 1.
[18] G.A. Schuler, T. Sjöstrand, Nucl. Phys. B 407 (1993) 539;
  G.A. Schuler, T. Sjöstrand, Z. Phys. C 73 (1997) 677;
  C. Bourrely, J. Soffer, T.T. Wu, Mod. Phys. Lett. A 15 (2000) 9;
  E. Gotsman et al., Eur. Phys. J. C 14 (2000) 511.
[19] B. Badelek, J. Kwiecinski, A.M. Stasto, Acta Phys. Pol. 30 (1999) 1807, hep-ph/0001161.
[20] P. Desgrolard et al., Eur. Phys. J. C 9 (1999) 623.

[21] OPAL Collaboration, K. Ackerstaff et al., Eur. Phys. J. C 14 (2000) 199.

[22] V.N. Gribov, I.Ya. Pomeranchuk, Phys. Rev. Lett. 8 (1962) 343;
S.J. Brodsky, J. Phys. Suppl. (Paris) 35 (1974) C2-69;
K.V.L. Sarma, V. Singh, Phys. Lett. B 101 (1981) 201.

[23] PLUTO Collaboration, Ch. Berger et al., Phys. Lett. B 149 (1984) 421;
TPC/2γ Collaboration, H. Aihara et al., Phys. Rev. D 21 (1990) 2667;
MD1 Collaboration, S.E. Baru et al., Z. Phys. C 53 (1992) 219.

[24] D. Cline, F. Halzen, J. Luthe, Phys. Rev. Lett. 31 (1973) 491.

[25] R.M. Godbole, G. Pancheri, Nucl. Phys. Proc. Suppl. 82 (2000) 246, hep-ph/0010104.

[26] A. Donnachie, H.G. Dosch, M. Rueter, Phys. Rev. D 59 (1999) 074011.